Metabolic investigation and auxiliary enzyme modelization of pyrrocidine pathway allow rationalization of paracyclophane-decahydrofluorene formation

Youwei Chen, Steffi Sewsurn, Séverine Amand, Caroline Kunz, Kevin Calabro, Didier Buisson, Stéphane Mann, Nicolas Pietrancosta

Metabolic investigation and auxiliary enzyme modelization of pyrrocidine pathway allow rationalization of paracyclophane-decahydrofluorene formation

Youwei Chen,[1] Steffi Sewsurn,[1] Séverine Amand,[1] Caroline Kunz,[1,2] Nicolas Pietrancosta,[3,4] Kevin Calabro,[1] Didier Buisson[1] and Stéphane Mann[1]*

[1] Laboratoire Molécules de Communication et Adaptation des Micro-organismes UMR 7245, Muséum national d'Histoire naturelle, CNRS, Sorbonne Universités ; CP54, 57 rue Cuvier, 75005 Paris, France.

[2] Sorbonne Université, Faculté des Sciences et Ingénierie, UFR 927, F-75005 Paris, France.

[3] Laboratoire des Biomolécules, LBM, Sorbonne Université, École Normale Supérieure, PSL University, CNRS, F-75005 Paris, France.

[4] Neurosciences Paris Seine - Institut de Biologie Paris Seine (NPS - IBPS), Sorbonne Université, INSERM, CNRS, F-75005 Paris, France.

*corresponding author.

Corresponding author for the journal: Stéphane Mann, E-mail: stephane.mann@mnhn.fr

Abstract:

Fungal paracyclophane-decahydrofluorene-containing natural products are complex polycyclic metabolites derived from similar hybrid PKS-NRPS pathways. Herein we studied the biosynthesis of pyrrocidines, one representative of this family, by gene inactivation in the producer *Sarocladium zeae* coupled to thorough metabolic analysis and molecular modelling of key enzymes. We characterized nine pyrrocidines and analogues as well as in mutants a variety of accumulating metabolites with new structures including rare cis-decalin, cytochalasan and fused 6/15/5 macrocycles. This diversity highlights the extraordinary plasticity of the pyrrocidine biosynthetic gene cluster. From accumulating metabolites, we delineated the scenario of pyrrocidine biosynthesis. The ring A of the decahydrofluorene is installed by PrcB, a membrane-bound cyclizing isomerase, on a PKS-NRPS derived pyrrolidone precursor. Docking experiments in PrcB allowed us to characterize the active site suggesting a mechanism triggered by arginine-mediated deprotonation at the terminal methyl of the substrate. Next, two integral membrane proteins, PrcD and PrcE, each predicted as four-helix bundle, perform hydroxylation of the pyrrolidone ring and paracyclophane formation, respectively. Modelisation of PrcE highlights a topological homology with vitamin K oxido-reductase and the presence of a disulphide bond. Our results suggest a previously unsuspected coupling mechanism via a transient loss of aromaticity of tyrosine residue to form the strained paracyclophane motif. Finally, the lipocalin-like protein PrcX drives the exo-cycloaddition yielding ring B and C of the decahydrofluorene to afford pyrrocidine A, which is transformed by a reductase PrcI to form pyrrocidine B. These insights will greatly facilitate the microbial production of pyrrocidine analogues by synthetic biology.

Introduction:

Pyrrocidines A **1** and B **2** (Fig. 1) are secondary metabolites isolated from diverse fungi[1–4] and characterized by antimicrobial[5] and apoptosis-inducing[6] activities, as well as potential inhibitory effects of SARS-CoV2 RNA-dependent RNA polymerase.[7] More importantly, pyrrocidines produced by the maize endophyte *Sarocladium zeae* (formerly classified as *Acremonium zeae*) are suggested to have a beneficial impact for the host plant, as sub-inhibitory concentrations of pyrrocidines can inhibit the fumonisin toxin production in the phytopathogen *Fusarium verticillioides*.[8,9] Pyrrocidines could thus be responsible, at least in part, for the protective effect of the producer in maize against phytopathogens. Pyrrocidines and analogues are therefore promising targets for the development of biocontrol agents. These molecules belong to a growing family of fungal natural products sharing a highly strained paracyclophane with a distorted aromatic ring connected to a decahydrofluorene core, which encompasses GKK1032A$_2$ **3**,[10] hirsutellone B **4**,[11] trichobamide A **5**,[12] xenoacremone C **6**, ascomylactams,[13,14] pyrrospirones[15] and embellicines.[16] These compounds attract much interest recently because of their diverse bioactivities (e.g. antimycobacterial, anti-glioma) and their complex structures. Each member possesses different combinations of configuration at the chiral centers present in the paracyclophane-decahydrofluorene motif, which represents a great challenge for chemical synthesis. This study is focused on the detailed understanding of pyrrocidine biosynthesis in *S. zeae*, in particular, the steps leading to polycyclic formation. Such knowledge will enable future pathway engineering efforts to generate pyrrocidine analogs with controlled stereochemistry.

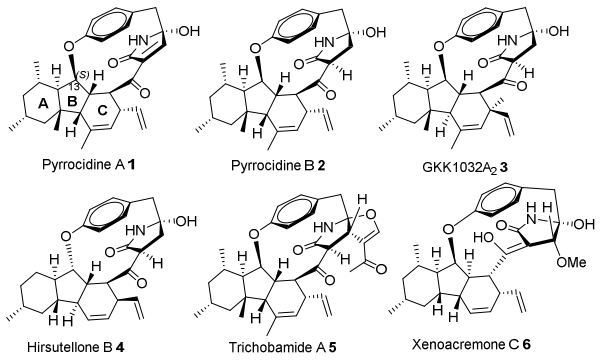

Figure 1: Pyrrocidine structures and related fungal para-cyclophane-decahydrofluorene metabolites.

The biosynthetic origin of this fungal scaffold was first studied by Oikawa[10] with isotopic incorporations of labelled acetate, L-tyrosine and methionine into GKK1032 biosynthesis. This suggested that a hybrid polyketide synthase – non-ribosomal peptide synthetase (PKS-NRPS) is involved. Later, feeding experiments on the maize endophyte *S. zeae* using dual labelling with ^{18}O,^{13}C L-tyrosine demonstrated the integration of the amino acid in pyrrocidines with conservation of the phenolic oxygen atom.[17] Consequently, chemical cascades were suggested to form the paracyclophane and decahydrofluorene motifs. The proposed reaction path (Scheme 1) involved a pyrrolidone key

intermediate I that results from the PKS-NRPS nonaketide-tyrosine product by Knoevenagel condensation, and an intermediate II containing the paracyclophane and ring A. Given the presence of a cyclohexene motif (ring C), an intramolecular Diels-Alder reaction (IMDA) would occur from the intermediate II in an *exo*- or *endo*-cyclizing way to form pyrrocidines or GKK1032A$_2$, respectively. Ohashi *et al.* heterologously expressed the biosynthesis pathways of pyrrocidine B **2** from *S. zeae* and GKK1032A$_2$ **3** from *Penicillium citrinum* in *Aspergillus nidulans*.[18] This work suggested that four proteins function together, likely as a complex, to transform intermediate I to II according to a mechanism involving the phenol oxygen attack on the olefinic C13 which then triggers the conjugated addition of C12 to the triene at C7 to form ring A. To note, this mechanism would result in a reverse configuration of (*S*)-C13 found in pyrrocidines and GKK1032A$_2$ which corresponds to that observed in hirsutellone B (Fig.1). Concurrent to this publication, Liu *et al.* characterized xenoacremones and their biosynthetic pathway in *X. sinensis*, and proposed that one enzyme (XenF) catalyses [1,11]-sigmatropic rearrangement to install ring A in intermediate III (Scheme 1).[19] Despite these proposed pathways for decahydrofluorene formation, the mechanism by which the paracyclophane is generated still remains an enigma.

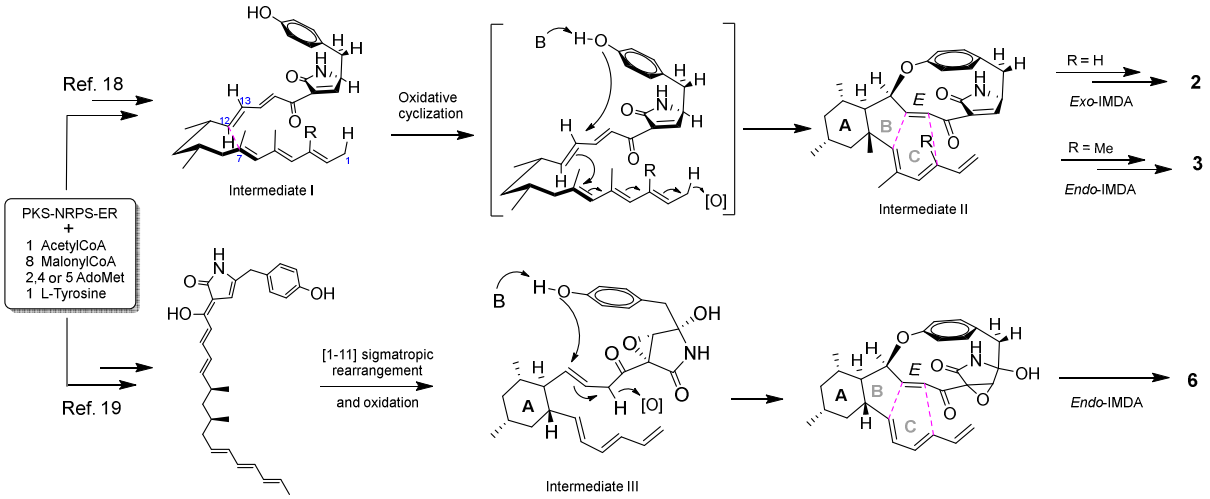

Scheme 1: Proposed intermediates in previous publications on the biosynthesis of pyrrocidine B, GKK1032A$_2$[18] or xenoacremones.[19] (IMDA: intramolecular Diels-Alder reaction)

In the present study, we investigated pyrrocidine biosynthesis in *S. zeae* by gene knock-out and thorough metabolic analysis. This reveals an intrinsic plasticity of the pyrrocidine pathway and leads to the generation of complex metabolites with new cyclic backbones in the mutants. Moreover, structural analysis of key auxiliary enzymes by modelling and of the products accumulated in respective gene knock-out strains allowed us to propose a plausible mechanism of paracyclophane formation.

Results and discussion

Pyrrocidine-related compounds in wild-type *S. zeae*.

Recent progress in the understanding of fungal natural product biosynthesis have suggested that fungal pathways are inherently capable of producing more than one compound from one pathway.[20] We therefore interrogated if this also holds true for pyrrocidine biosynthesis. The fungi *S. zeae* was cultivated on PDA medium for seven days and the ethyl acetate metabolite extracts were analyzed by liquid chromatography coupled to high resolution mass spectrometry (LC-HR-MS). Pyrrocidines A **1** and B **2** were detected at 15.8 min and 15.9 min ($[M+H]^+$ ions at *m/z* 488.2795 and 490.2952), respectively (Fig S5; for detailed NMR characterizations see Tables S5, S6). Careful analysis of the extracted ion chromatogram (EIC) of *m/z* 490.2952 showed two other small peaks, namely compounds **7a** at 15.5 min and **7b** at 14.9 min. Interestingly, these two compounds accumulated significantly compared to **1** and **2** in the culture on maize medium for 30 days**,** enabling access to sufficient amounts for isolation (Fig S13). Structural characterization by NMR (ESI and Tables S7-9) showed that compound **7a** is a diastereomer of **2** at position C3 and C6, whereas **7b** is the enol form of **7a** at C16 (Fig. 2). Both compounds resulted from *endo*-type IMDA cyclization. Moreover, pyrrocidine C **9**[5,17] ($[M+H]^+$ at *m/z* 504.2744, RT 15.5 min) and epi-pyrrocidine A[3] ($[M+H]^+$ at *m/z* 488.2795, RT 15.0 min), named here pyrrocidine F **11**, were also detected by LC-MS. Their structure was confirmed by NMR (Tables S11, S13). In addition, a new compound with the molecular formula (MF) $C_{35}H_{41}NO_5$ ($[M+H]^+$ at *m/z* 556.3057 obs., Fig. S13) identical to that of trichobamide A **5**[12] was isolated. NMR analysis showed that it is an isomer of **5** differing in the substitution of the tetrahydrofuro-pyrrolone moiety at C33 and C34, that we named trichobamide B **8** (Fig. 2, Table S10; for proposed biosynthesis of **5** and **8** see Scheme S5).

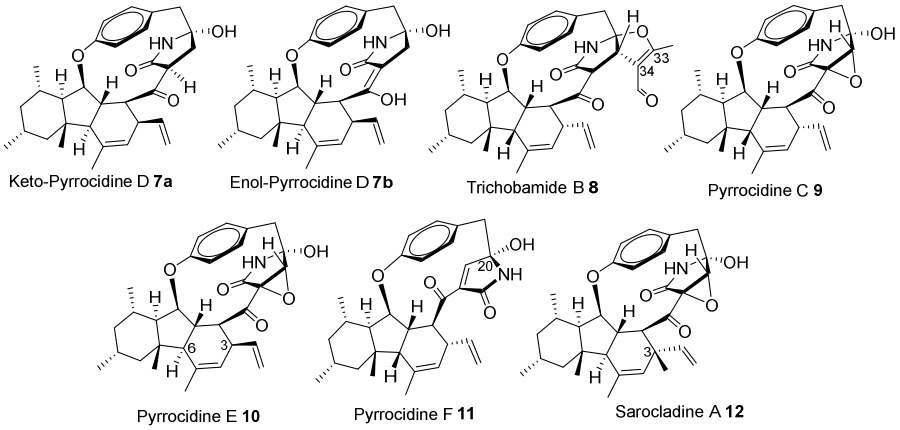

Figure 2: Analogues of pyrrocidines isolated and characterized from *Sarocladium zeae* in this study.

Function of genes whose deletion still leads to pyrrocidine scaffold

To identify the biosynthetic gene cluster (BGC) of pyrrocidines, we constructed a genomic library, sequenced the genome of *S. zea*e and subsequently identified three potential PKS-NRPS gene

clusters. We then established protocols for gene inactivation in *S. zeae*, based on allelic exchange with a hygromycin resistant cassette by homologous recombination, using protoplastization and PEG-mediated transformation[21] (ESI and Fig. S1-4). Inactivation of the PKS-NRPS genes of each cluster allowed to assign the cluster responsible for pyrrocidine biosynthesis named *prc* (Fig. 3A, S6). Sequence analysis predicted that the *prc* cluster contains 11 genes encoding a PKS-NRPS (PrcA), a Diels-Alderase (PrcB), two *trans*-acting enoyl reductases (ER; PrcC and I), an α,β-hydrolase (PrcH), two transcription factors (PrcF and J), a transporter (PrcG), a lipocaline-like protein of unknown function (PrcX) and two integral membrane proteins (PrcD and E). Genome mining revealed thirteen similar BGCs in the sequenced fungi databases (Fig. S16). To assign a precise function to each post-PKS/NRPS protein encoded by the BGC, we generated single gene knock-out strains of *S. zeae*. Extracts of the mutants were analyzed by LC-HR-MS and accumulated products were purified from maize cultures (Tables S2-4) and characterized by NMR analysis.

First, given the weaker similarity of PrcI to ER, we reasoned that it is involved in the reduction of pyrrocidine A **1** to form B **2**, instead of acting as a canonical ER of PKS-NRPS. Indeed, the deletion of *prcI* abolished the production of pyrrocidines B **2** and D **7a,b,** but not pyrrocidine A **1** (Fig. 3B and S8).

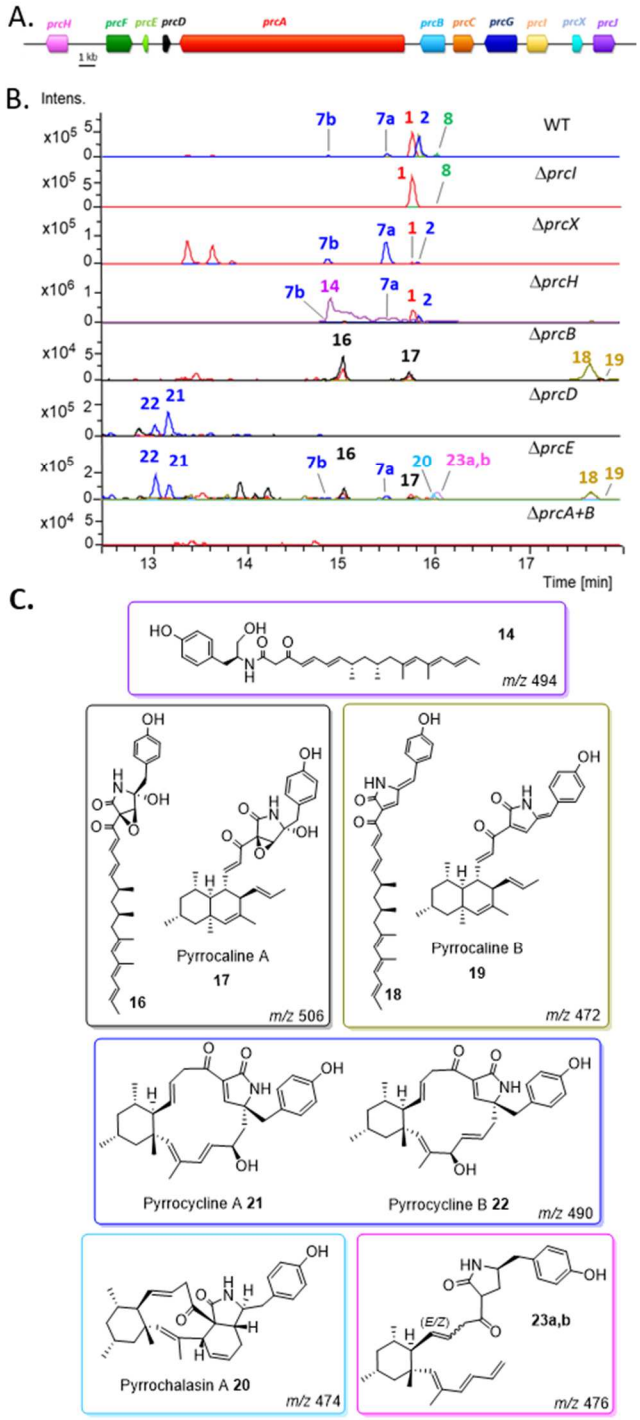

Figure 3. A. Biosynthetic gene cluster (*prc*) of pyrrocidines in *Sarocladium zeae*. B. LC-MS analysis of metabolite extracts from wild type (WT) and deletion mutants of *S. zeae*. Superimposed EIC: *m/z* 490.295 (dark blue), 488.279 (red), 556.306 (green), 494.326 (violet), 506.290 (black), 476.316 (pink), 474.300 (blue) for each deletion mutants and wild type *S. zeae*. C. Structures of isolated metabolites.

Next, deletion of *prcX* (lipocaline-like protein) led to a strong decrease of **1** and **2** production, without impacting the formation of pyrrocidines D **7a,b** (Fig. 3B and S9). This result shows that **1** and **2** can be formed without PrcX. This protein thus controls the Diels-Alder cycloaddition in favor of the *exo* product from precursor **26** (Scheme 2, Fig. S2), but is not indispensable in this process. Moreover,

from maize culture (Fig. S14) we could detect a new compound named pyrrocidine E **10** (MF $C_{31}H_{37}NO_5$; $[M+H]^+$ *m/z* 504.2736, RT 15.4 min), whose structure was assigned to the C3, C6 diastereomer of pyrrocidine C **9** by NMR (Fig. 2, Table S12). It can be resulted from epoxidation of **27**, which is the equivalent of **1** from *endo*-type cyclization (Schemes 2 and S2). Intriguingly, the strong decrease of **1** and **2** in *ΔprcX* mutant enabled the isolation of a previously-unidentified metabolite **12** (MF $C_{32}H_{39}NO_5$; $[M+H]^+$ *m/z* 518.2901, RT 16.0 min)**,** named sarocladine A. Subsequent re-examination of the wild-type strain also revealed the presence of **12**. The structure of **12** was characterized as the C3-epimer of GKK1032C.[22] Indeed, NOESY spectrum through the cross-correlations H31-H24-H13-H6-H12-H15, H13-H15-H1a-H6 and H14-H26-H29 showed that H12, H13, H15, H6, methyl 31 and the vinyl group are cofacial, while H14 and methyl 29 are on the opposite face of the decahydrofluorene (Table S14). The *trans*-fused junction of rings B and C in both **10** and **12** was corroborated by the shielding of C7, C28 and C29 chemical shifts (as in **7a,b**, see ESI). The formation of **12** indicates that PrcA is able to perform four and five methylations on the elongating polyketide chain, respectively, which is to our knowledge the first reported example for a fungal PKS-NRPS. Moreover, the inverse configuration of C3 in sarocladine A **12**, compared to other endo-cyclized products (i.e. **7a,b**, **10**), suggests an influence on the stereochemical control by the methylation event during post-PKS-NRPS processes.

When *prcH* encoding the α,β-hydrolase was inactivated, pyrrocidine production was not impaired (Figure 3B and S7). BLAST search in the genome confirmed the absence of another copy of *prcH* and homologous genes. In addition, compound **14** (MF $C_{31}H_{43}NO_4$; $[M+H]^+$ *m/z* 494.3297), an all-*E* polyene alcohol, accumulated in the extract (Scheme 2, Table S15). **14** is conceivably a shunt product that is formed *via* further reduction of a putative aldehyde intermediate **13**, released from the PKS-NRPS by the terminal reduction domain. This result is consistent with previous reports on other fungal PKS-NRPS BGCs[23,24] in which α,β-hydrolases were inactivated. Moreover, the non-essentiality of PrcH in pyrrocidine production could be attributed to the spontaneous Knoevenagel condensation of the aldehyde **13** (Scheme 2). Aldehyde evaded detection in the extract, likely due to fast conversions in alcohol or pyrrolidone derivatives. Cox and coworkers provided evidence to this scenario using synthetic aldehyde compounds and enzymatic assay in a related PKS-NRPS pathway.[25,26] These results suggest that the role of PrcH is to prevent the reduction of the PKS-NRPS off-loaded reactive aldehyde **13** in order to promote its ring closing into pyrrolidone **15** through a Knoevenagel condensation.

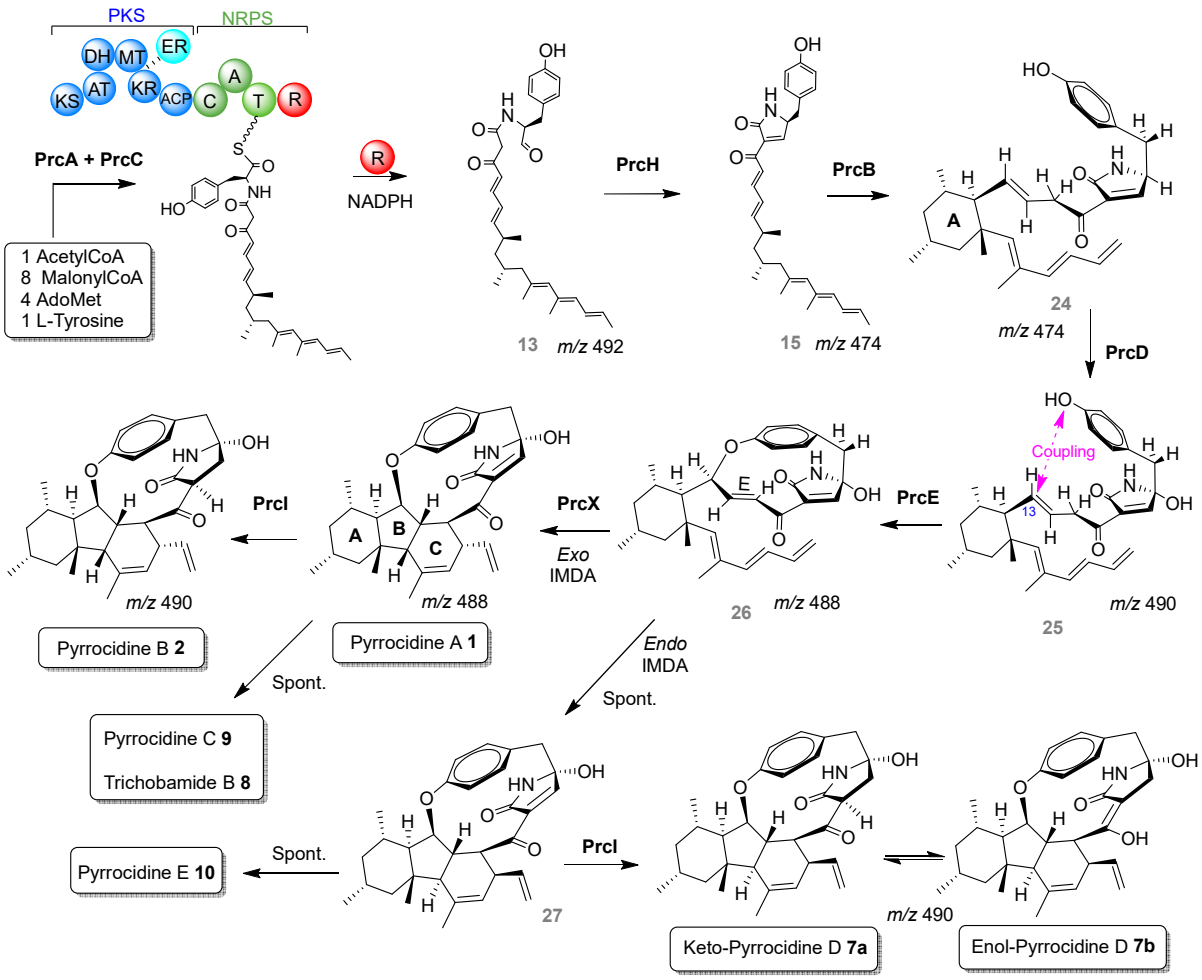

Scheme 2: Proposed biosynthesis pathway of pyrrocidines in *Sarocladium zeae*. Isolated compounds are framed while non-isolated intermediates appear with a grey numbering.

Function of genes involved in the paracyclophane-decahydrofluorene formation

Individual disruptions of *prcB, D and E* genes led to accumulation of compounds with novel ring structures. In *ΔprcB* mutant, the production of pyrrocidines is abolished and we observed the formation of **16** and **17** with MF of $C_{31}H_{39}NO_5$ ($[M+H]^+$ of *m/z* 506.289; RT at 14.9 and 15.8 min, respectively) (Fig. 3B, S10). Structure elucidation showed that **16** is a 5-hydroxy-3,4-epoxy-pyrrolidone substituted with a linear polyolefinic chain as in **14**. Compound **17** is a *cis*-decalin with a relative stereochemistry deduced from NOESY data by the cross correlations H12-H29-H10b-H14-H15-H4 (Table S16-17). It can be resulted from **16** by an *exo*-selective IMDA (Scheme S1). The couple of compounds **18** and **19** were also detected, at a higher retention time (17.6 and 17.8 min, respectively). Similarly to the couple **16** and **17,** structure assignments (MF of $C_{31}H_{37}NO_3$ with $[M+H]^+$ of *m/z* 472.283) show a polyolefinic system and a *cis*-decalin for **18** and **19**, respectively (NMR tables S23, S24, Scheme S1).

Several shunt products accumulated in Δ*prcE* mutant (Fig. 3B, S12), in addition to **16, 17, 18** and **19**. Compound **20** (MF $C_{31}H_{39}NO_3$; $[M+H]^+$ *m/z* 474.2998; RT 15.8 min) was revealed to have a unique 6/10/6/5 fused polycyclic structure substituted by a tyrosine residue by NMR (Table S18). This macrocycle fused to an amino acid-derived octahydro-isoindole resembles cytochalasans.[27] **20** was thus named pyrrochalasin A and represents the first nonaketide-tyrosine member of this family. Its relative stereochemistry was assigned by NOESY experiment, on the base of two identified groups of cross correlations H30-H10b-H31-H12-H14-H28 and H29-H6-H4-H19-H23, which indicates that these groups of protons are respectively on each side of the equatorial plan of the molecule. Furthermore, two other cyclic compounds with a MF of $C_{31}H_{39}NO_4$ ($[M+H]^+$ *m/z* 490.293 obs.), named pyrrocyclines A **21** and B **22,** were detected at RT 13.2 and 13.0 min, respectively. Their planar structures were established showing a unique backbone consisting of a 15-membered macrocycle fused to 6- and 5-membered rings. NOESY spectra indicated that they adopt a conformation in which protons H14, H12, H6, H8, H4, H2 and NH are oriented on the same face of the equatorial plan of the molecule, while H23/27, H21, H19, H1 H3, H28, H29, H13, H11 are located on the opposite face (Tables S19-20). **21** and **22** differ from each other at the position of the hydroxyl group. Trimethyl-cyclohexane-containing compounds **23** (MF $C_{31}H_{41}NO_3$; $[M+H]^+$ *m/z* 476.3146 obs.; RT 16.0 min) were also isolated and NMR analysis revealed that **23** is a mixture of two *E*/*Z* isomers of C13-C14 olefin in a 1:1 ratio (measured coupling constants: **23a** ^3J_E = 15.3 Hz and **23b** ^3J_Z = 9.3 Hz) (Tables S21-22). Note that a conjugated trienic chain substituting the trimethyl-cyclohexane motif was isomerized at the C1 terminal position in **23**, unlike the polyketide part in **14, 16** and **18**. In addition to these new compounds, Δ*prcE* produces pyrrocidines D **7a,b** and few amounts of B **1** but not A **2** neither its derivatives **8** or **9**. On the contrary, deletion of *prcD* led to few accumulated products. Only macrocycles **21** and **22** were present in Δ*prcD* mutant (Fig. S11).

Given that the accumulating metabolites from Δ*prcE* or Δ*prcD* harbor the trimethyl cyclohexane motif (ring A), whereas those observed in the Δ*prcB* mutant do not, PrcB is proposed to install ring A with an isomerization-cyclization step from pyrrolidone **15** to the key intermediate **24**. Isolation of compounds **20**, **21** and **22** provides strong support for the intermediacy of **24** (Scheme 2, Fig. S15). Indeed, **19** can gives rise to **20** in Δ*prcE* through an *endo*-selective IMDA as in the biosynthesis of cytochalasans. It is to mention that such a stereocontrolled cyclization required a pericyclase as demonstrated by Hantke *et al.* in pyrichalasin H biosynthesis.[27] This suggests that the formation of **20** is not spontaneous and may be governed by a protein like PrcX (Scheme S3). Macrocyclization of **24** after epoxidation at C1-C2 or C3-C4 olefins can provide the compounds **21** and **22** (Scheme S4).

The formation of **16** and **17** can be explained by C20 hydroxylation of **15** followed by spontaneous either dehydration or epoxidation, respectively (Scheme S1). Such autooxidation of

strained olefins to form epoxides has been previously reported[28] and is also exemplified by the known spontaneous conversion of **1** to **9.**[5,17] Metabolite profile comparison of all the mutants showed that shunt products **16, 17, 18** and **19** are absent when *prcD* is inactivated (Fig. S7-S12). This indicates that PrcD is involved in hydroxylation of the pyrrolidone moiety. Taken together, we deduced that PrcD hydroxylates **24** to give **25** (Scheme 2). PrcE next installs paracyclophane motif on **25** to give **26**, which undergoes an *exo* IMDA assisted by PrcX to afford **1**. By contrast, in Δ*prcE* mutant the formation of paracyclophane in **7** and **2** may occur from the enol form of **25** by the O-attack of phenol on C13 (Scheme S5). Concomitant rearrangement of the Pi-system with protonation at C19 installs the C14-C15 double bound required for the next IMDA reactions directly supplying pyrrocidines D and B. Moreover, complementation of Δ*prcE* mutant with *prcE* gene restored the production of pyrrocidine A (Figure S15). Consequently, the formation of pyrrocidines B and D but not pyrrocidine A in Δ*prcE* mutant corroborates our proposed biosynthetic pathway *via* intermediate **26**.

Genes *prcE, D* and *B* were separately cloned for heterologous expression in *E. coli*. However, protein inductions show cell toxicity for PrcE and D and led to a low solubility of PrcB, very likely due to the membrane nature of these proteins. Metabolites **24**, **17** and **23** when tested as substrates of PrcB or in biotransformations with Δ*prcE or* Δ*prcB* mutants were not transformed. Therefore, we turned towards *in silico* analysis of the proteins for understanding the molecular basis of their mechanisms.

Tridimensional model of PrcB and docking calculations with the biosynthetic intermediate 15.

Sequence alignments of PrcB show that its closest homologs with identified functions belong to the fungal decalin synthases (DS) family like CghA, Fsa2 and Phm7 (21%, 22% and 24% sequence identities, respectively; Fig. S18). These three proteins all adopt the same fold made of a N-terminus β-sandwich domain connected by a short α-helix to a C-terminus β-barrel domain as revealed by recent crystal structure resolutions.[29–31] The DS active sites are located in the cavity formed at the interface of these two domains. Noteworthily, compared to the characterized DSs, PrcB has extended sequences that are predicted to form α-helixes at both of its extremities (Fig. S17); this feature is conserved in all PrcB homologs found in pyrrocidine-like BGCs (Fig. S16). The N-terminus helix of PrcB (residues 5-22) has the signature of a transmembrane segment, which suggests PrcB is anchored in the membrane and likely forms a complex with the integral transmembrane proteins PrcD and PrcE, enabling to channel reactive intermediates up to the end product.

In order to investigate the catalytic mechanism of PrcB, we modelized this protein according to the crystal structure of CghA and performed docking calculations with substrate **15**. An active site pocket at the interface of the two domains was delineated. We obtained several similar poses of **15**

fitting the cavity in which the molecule adopts an elbow shape with the phenoxy group anchored in a calix made of four tryptophan residues (Trp81, Trp254, Trp261, Trp276) and Leu248. The hydrocarbon chain from C7 to C12 is preorganized in a chair-like conformation, with the C30 and C31 methyls in equatorial positions and C29 in an axial position as in the ring A. This part of the molecule interacts with residues Tyr120, Tyr360, Met362, Met370 and Leu132 (Fig. 4 and S22). In the vicinity of the C12-C15 diene we also identified the presence of the residue Glu118. Interestingly, the terminal methyl C1 points towards the guanidinium of Arg265 which interacts with both carboxylates of Asp87 and Glu85 *via* a salt bridge and charge-charge interaction, respectively. All these residues involved in the binding pocket are conserved in PrcB homologs found in pyrrocidine BGCs (Fig. S17).

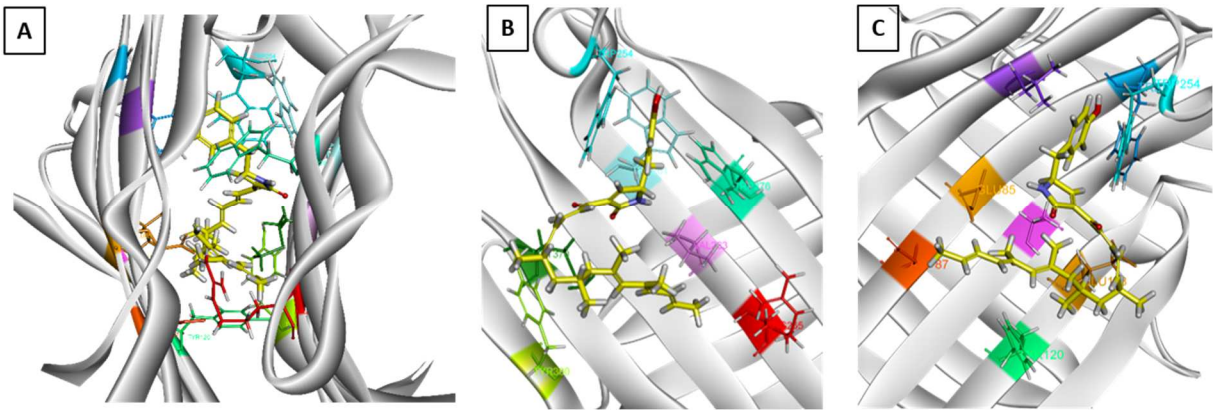

Figure 4. Docking of the intermediate **15** adopting a C14-C15 *s-trans* conformation in modelized PrcB: A. View of **15** (in yellow) in the pocket localized at the interface of both N- and C-terminal domains; B. View of the interactions of **15** with C-terminal domain residues (Arg265 red, Val263 pink, Tyr254 and Tyr261 cyan, Tyr276 spring green, Tyr360 green, Met370 dark green); C. View of the interactions of **15** with the N-terminal domain residues (Trp81 blue, Trp254 cyan, Leu248 violet, Tyr120 green, Asp87 orange, Glu85 ochre yellow, Glu118 brown).

This model allowed us to propose a plausible cyclization mechanism for ring A formation. Given the interaction of C1 and Arg265, we proposed that Arg265 activated by Glu85 and Asp87 deprotonates C1 and initiates the isomerization of double bonds along the chain. This would trigger the attack of C7 from its *si* face onto the *si* face of C12 to afford ring A after protonation of C15 by Glu118 (Fig. S22). Arginine residues are known to act as general base catalysts in various enzymes in which the guanidinium is activated through an interaction network with carboxylate groups from other residues.[32,33] Noteworthily, this tetrad of residues is specific to and conserved in all PrcB homologs of pyrrocidine BGCs but not in DSs, in which either Arg265 (CghA, Fsa2) or Glu85/Glu118 (Phm7) are present (Fig. S17-18). Furthermore, among the different docking poses of substrate **15**, the C13-C14 bond adopts either *s-trans* (most of the cases) or *s-cis* conformation. By the cyclo-isomerization mechanism we proposed, these conformers would generate the (13-14)-*E*-alkene **24** and its (13-14)-*Z* isomer **28**, accounting for the formation of isolated compounds **23a,b** (Scheme 3). Our PrcB model

showing that the C1 and C15 in **15** are strongly distanced in the cavity (*ca.* 10 Å) does not support a [1,11] sigmatropic rearrangement, as speculated in the process of xenoacremone biosynthesis[19] with XenF (80.2 % sequence identity with PrcB) and where the required cyclic transition state should bring these carbons closer for H migration.

Proposed mechanism of paracyclophane formation

Sequence analysis of PrcD and PrcE with various bioinformatic tools (Fig. S23-28)[34–36] allowed us to classify both protein in the four transmembrane (TM) protein family which encompasses a large diversity of topologies and functions.[37] The TM architecture of PrcD (Fig. S19) resembles that of connexin,[38] but no enzymatic function was identified for this TM family allowing to propose a hydroxylation mechanism for PrcD. By contrast, the topology of PrcE (Fig. S20) which harbors a 30-residue loop between TM1 and TM2 structured as a short α-helix and a strand, is similar to that of vitamin K epoxide reductase (VKOR)[39,40] and disulfide bond formation protein DsbB.[41,42] These enzymes commonly use cysteine pairs as active site residues to reduce a quinone (vitamin K in VKOR and ubiquinone or menaquinone in DsbB) to its hydroquinone form, by switching between reduced and disulfide-bridged states. In this process, one of the cysteines covalently binds to the substrate to form a transient cysteine-quinone adduct. Indeed, PrcE possesses a unique pair of cysteines positioned almost in the middle of TM1 (Cys22) and TM4 (Cys114), facing each other in a way allowing a disulfide bond formation inside the four-helix bundle scaffold (Fig. S26). This was confirmed by our PrcE model showing a stable disulfide bridge (Figure 5).

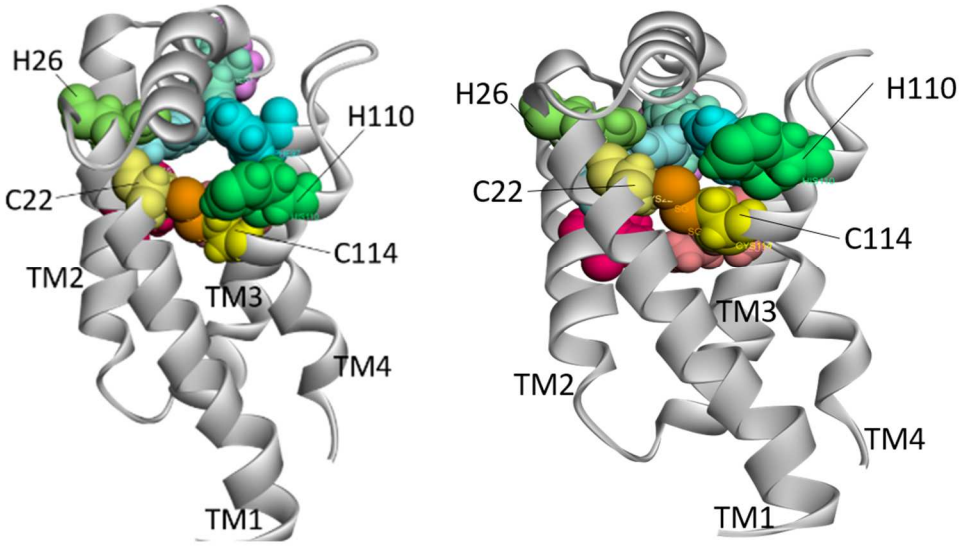

Figure 5. Modelized PrcE with C22-C114 disulfide bond (Cysteins: yellow, sulfur atoms: orange). Four TM segments are located at residues 10-29 (TM1), 60-78 (TM2), 84-104 (TM3) and 107-123 (TM4).

Inspired by the mechanism of VKOR and DsbB, we reasoned that PrcE can use disulfide bond as electron acceptor in the oxidative step of paracyclophane formation *via* a transient cysteine-quinone adduct formed between C22 of the intermediate **25** and sulfur of one of the active site cysteines (Scheme 3). The resulting introduction of *sp3* hybridization on carbon C22 and the loss of aromatization releases the chain constrain allowing C13 and the oxygen of the transient quinone to come closer. Next, the attack of C13 on the quinone oxygen would occur to close the ring with liberation of cysteine residue and restoration of aromaticity resulting in a trapped distorted benzene ring. This reactivity is supported by the work of Guo & Mayr reporting the O-electrophilicity of activated quinones towards Pi-nucleophiles.[43] This attack can be triggered by the abstraction of a proton at C15 to generate the *E*-C14-C15 double bond of **26** required for the subsequent IMDA step. Taken together, backed by in silico analysis of PrcE, the proposed mechanism of paracyclophane formation involving a transient dearomatization step bypasses the energetic constraint inherent to the distorted aromatic ring found in pyrrocidines, and provides for the first time a plausible insight into this process.

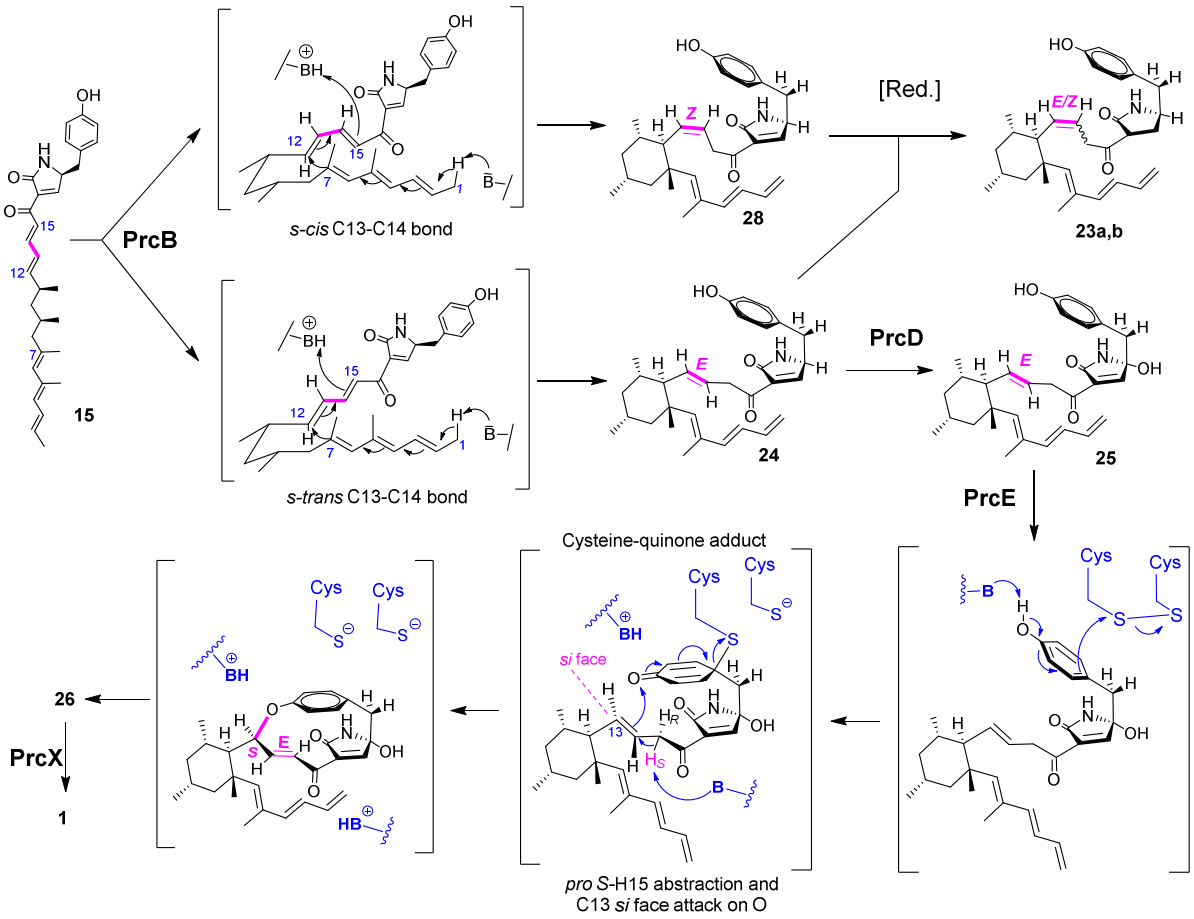

Scheme 3. Proposed mechanism for the formation of the paracyclophane-decahydrofluorene of pyrrocidine A **1** involving PrcB,D,E and X. C13-C14 σ-bond of intermediate **15** adopts a *s-cis* or *s-trans* conformation in PrcB giving rise to *E*-**24** or *Z*-**28** intermediates after double bond displacement. Accumulation of **23a,b** in *ΔprcE* mutant resulted in reduction of the double bond in pyrrolidone moiety.

Conclusions

Herein, applying gene inactivation coupled to thorough metabolic analysis and protein modelling, we were able to draw a biosynthetic pathway for pyrrocidines and propose a mechanism for paracyclophane-decahydrofluorene formation involving a membrane bound protein sequence. This work underlines the extraordinary plasticity of the pyrrocidine pathway, illustrating perfectly the intrinsic property of "one pathway, many compounds". Altogether, these insights provide a blueprint for future engineering efforts allowing pathways to generate valuable pyrrocidine analogues.

Author Contributions

SM: project conception and funding; DB and SM: supervision; YC, SS, SA, CK, NP, DB, SM: experiments; YC, SS, SA, CK, NP, KC, DB, SM: data analysis. SM wrote the paper with input from all authors.

Conflicts of interest

There are no conflicts to declare.

Supporting information

General procedures and materials, experimental details including generation and characterization of *S. zeae* mutants, protein sequence alignments and modelizations; LC-MS data of metabolite extracts of the mutants and wild type of *S. zeae*; ^{1}H and ^{13}C NMR data for all isolated compounds including 1D and 2D spectra; proposed biosynthetic pathways of compounds **5**, **8**, **12**, **17**, **19**, **20**, **21**, **22** and **27**.

Acknowledgements

Y. Li and B. Nay are thanked for initiating the project of genome sequencing, and R. Müller and his group for assistance in the construction of genomic DNA library. We thank A. Delporte, N. Dallel and D. Barbash who contributed to the project during their internship, A. Blond and A. Deville from the NMR service of MHNH and A. Marie and R. Puppo from the mass spectrometry service of MNHN. The NMR and LC-Mass spectrometers used in this study were funded jointly by the Région Ile-de-France, the MNHN (Paris, France) and the CNRS (France). This work was supported by IDEX Sorbonne Universités as Emergence Project (grant number SU-15-R-EMR-19-1, FungiMIP), by MNHN (ATM funding 2019-2020, PolyFungID). We thank the China Scholarship Council for granting Y. Chen (grant number 201808350098), and the French Ministry of Research for the Ph.D fellowship of S. Sewsurn and Sorbonne University (ED406).

References

(1) He, H.; Yang, H. Y.; Bigelis, R.; Solum, E. H.; Greenstein, M.; Carter, G. T. Pyrrocidines A and B, New Antibiotics Produced by a Filamentous Fungus. *Tetrahedron Lett.* **2002**, *43* (9), 1633–1636. https://doi.org/10.1016/S0040-4039(02)00099-0.

(2) Wicklow, D. T.; Poling, S. M.; Summerbell, R. C. Occurrence of Pyrrocidine and Dihydroresorcylide Production among Acremonium Zeae Populations from Maize Grown in Different Regions. *Can. J. Plant Pathol.* **2008**, *30* (3), 425–433. https://doi.org/10.1080/07060660809507540.

(3) Shiono, Y.; Furukawa, M.; Koseki, T.; Kwon, E.; Kurniawan, A. H.; Sato, S.; Harneti, D.; Maharani, R.; Supratman, U.; Uesugi, S.; Kimura, K. A Pyrrocidine Derivative Produced by Fungus Neonectria Ramulariae In-2 Isolated from a Beetle Holotrichia Picea. *Phytochem. Lett.* **2018**, *26*, 120–124. https://doi.org/10.1016/j.phytol.2018.05.030.

(4) Błaszczyk, L.; Waśkiewicz, A.; Gromadzka, K.; Mikołajczak, K.; Chełkowski, J. Sarocladium and Lecanicillium Associated with Maize Seeds and Their Potential to Form Selected Secondary Metabolites. **2021**, 11. https://doi.org/10.3390/biom11010098.

(5) Wicklow, D. T.; Poling, S. M. Antimicrobial Activity of Pyrrocidines from Acremonium Zeae Against Endophytes and Pathogens of Maize. *Phytopathology* **2009**, *99* (1), 109–115. https://doi.org/10.1094/PHYTO-99-1-0109.

(6) Uesugi, S.; Fujisawa, N.; Yoshida, J.; Watanabe, M.; Dan, S.; Yamori, T.; Shiono, Y.; Kimura, K. Pyrrocidine A, a Metabolite of Endophytic Fungi, Has a Potent Apoptosis-Inducing Activity against HL60 Cells through Caspase Activation via the Michael Addition. *J. Antibiot. (Tokyo)* **2016**, *69* (3), 133–140. https://doi.org/10.1038/ja.2015.103.

(7) Ebrahimi, K. S.; Ansari, M.; Hosseyni Moghaddam, M. S.; Ebrahimi, Z.; salehi, Z.; Shahlaei, M.; Moradi, S. In Silico Investigation on the Inhibitory Effect of Fungal Secondary Metabolites on RNA Dependent RNA Polymerase of SARS-CoV-II: A Docking and Molecular Dynamic Simulation Study. *Comput. Biol. Med.* **2021**, *135*, 104613. https://doi.org/10.1016/j.compbiomed.2021.104613.

(8) Wicklow, D. T.; Roth, S.; Deyrup, S. T.; Gloer, J. B. A Protective Endophyte of Maize: Acremonium Zeae Antibiotics Inhibitory to Aspergillus Flavus and Fusarium Verticillioides1 1Dedicated to John Webster on the Occasion of His 80th Birthday. *Mycol. Res.* **2005**, *109* (5), 610–618. https://doi.org/10.1017/S0953756205002820.

(9) Gao, M.; Glenn, A. E.; Gu, X.; Mitchell, T. R.; Satterlee, T.; Duke, M. V.; Scheffler, B. E.; Gold, S. E. Pyrrocidine, a Molecular off Switch for Fumonisin Biosynthesis. *PLOS Pathog.* **2020**, *16* (7), e1008595. https://doi.org/10.1371/journal.ppat.1008595.

(10) Oikawa, H. Biosynthesis of Structurally Unique Fungal Metabolite GKK1032A2: Indication of Novel Carbocyclic Formation Mechanism in Polyketide Biosynthesis. *J. Org. Chem.* **2003**, *68* (9), 3552–3557. https://doi.org/10.1021/jo0267596.

(11) Isaka, M.; Rugseree, N.; Maithip, P.; Kongsaeree, P.; Prabpai, S.; Thebtaranonth, Y. Hirsutellones A–E, Antimycobacterial Alkaloids from the Insect Pathogenic Fungus Hirsutella Nivea BCC 2594. *Tetrahedron* **2005**, *61* (23), 5577–5583. https://doi.org/10.1016/j.tet.2005.03.099.

(12) Chen, S.; Shen, H.; Zhang, P.; Cheng, H.; Dai, X.; Liu, L. Anti-Glioma Trichobamide A with an Unprecedented Tetrahydro-5 *H* -Furo[2,3- *b*]Pyrrol-5-One Functionality from Ascidian-Derived Fungus *Trichobotrys Effuse* 4729. *Chem. Commun.* **2019**, *55* (10), 1438–1441. https://doi.org/10.1039/C8CC08970A.

(13) Chen, Y.; Liu, Z.; Huang, Y.; Liu, L.; He, J.; Wang, L.; Yuan, J.; She, Z. Ascomylactams A–C, Cytotoxic 12- or 13-Membered-Ring Macrocyclic Alkaloids Isolated from the Mangrove Endophytic Fungus *Didymella* Sp. CYSK-4, and Structure Revisions of Phomapyrrolidones A and C. *J. Nat. Prod.* **2019**, *82* (7), 1752–1758. https://doi.org/10.1021/acs.jnatprod.8b00918.

(14) Wang, L.; Huang, Y.; Huang, C.; Yu, J.; Zheng, Y.; Chen, Y.; She, Z.; Yuan, J. A Marine Alkaloid, Ascomylactam A, Suppresses Lung Tumorigenesis via Inducing Cell Cycle G1/S Arrest through ROS/Akt/Rb Pathway. *Mar. Drugs* **2020**, *18* (10), 494. https://doi.org/10.3390/md18100494.

(15) Song, T.; Chen, M.; Chai, W.; Zhang, Z.; Lian, X.-Y. New Bioactive Pyrrospirones C–I from a Marine-Derived Fungus Penicillium Sp. ZZ380. *Tetrahedron* **2018**, *74* (8), 884–891. https://doi.org/10.1016/j.tet.2018.01.015.

(16) Ebrahim, W.; Aly, A. H.; Wray, V.; Mándi, A.; Teiten, M.-H.; Gaascht, F.; Orlikova, B.; Kassack, M. U.; Lin, W.; Diederich, M.; Kurtán, T.; Debbab, A.; Proksch, P. Embellicines A and B: Absolute Configuration and NF-κB Transcriptional Inhibitory Activity. *J. Med. Chem.* **2013**, *56* (7), 2991–2999. https://doi.org/10.1021/jm400034b.

(17) Ear, A.; Amand, S.; Blanchard, F.; Blond, A.; Dubost, L.; Buisson, D.; Nay, B. Direct Biosynthetic Cyclization of a Distorted Paracyclophane Highlighted by Double Isotopic Labelling of L-Tyrosine. *Org. Biomol. Chem.* **2015**, *13* (12), 3662–3666. https://doi.org/10.1039/C5OB00114E.

(18) Ohashi, M.; Kakule, T. B.; Tang, M.-C.; Jamieson, C. S.; Liu, M.; Houk, K. N.; Tang, Y. Biosynthesis of Para-Cyclophane Containing Hirsutellone-Family of Fungal Natural Products. 71. https://doi.org/10.1021/jacs.1c00098.

(19) Liu, Z.; Li, W.; Zhang, P.; Fan, J.; Zhang, F.; Wang, C.; Li, S.; Sun, Y.; Chen, S.; Yin, W. Tricarbocyclic Core Formation of Tyrosine-Decahydrofluorenes Implies a Three-Enzyme Cascade with XenF-Mediated Sigmatropic Rearrangement as a Prerequisite. *Acta Pharm. Sin. B* **2021**, S2211383521001064. https://doi.org/10.1016/j.apsb.2021.03.034.

(20) Wasil, Z.; Pahirulzaman, K. A. K.; Butts, C.; Simpson, T. J.; Lazarus, C. M.; Cox, R. J. One Pathway, Many Compounds: Heterologous Expression of a Fungal Biosynthetic Pathway Reveals Its Intrinsic Potential for Diversity. *Chem. Sci.* **2013**, *4* (10), 3845–3856. https://doi.org/10.1039/C3SC51785C.

(21) Hamada, W.; Reignault, P.; Bompeix, G.; Boccara, M. Transformation of Botrytis Cinerea with the Hygromycin B Resistance Gene, Hph. *Curr. Genet.* **1994**, *26* (3), 251–255. https://doi.org/10.1007/BF00309556.

(22) Qi, X.; Li, X.; Zhao, J.; He, N.; Li, Y.; Zhang, T.; Wang, S.; Yu, L.; Xie, Y. GKK1032C, a New Alkaloid Compound from the Endophytic Fungus Penicillium Sp. CPCC 400817 with Activity against Methicillin-Resistant S. Aureus. *J. Antibiot. (Tokyo)* **2019**, *72* (4), 237–240. https://doi.org/10.1038/s41429-019-0144-5.

(23) Sato, M.; Dander, J. E.; Sato, C.; Hung, Y.-S.; Gao, S.-S.; Tang, M.-C.; Hang, L.; Winter, J. M.; Garg, N. K.; Watanabe, K.; Tang, Y. Collaborative Biosynthesis of Maleimide- and Succinimide-Containing Natural Products by Fungal Polyketide Megasynthases. *J. Am. Chem. Soc.* **2017**, *139* (15), 5317–5320. https://doi.org/10.1021/jacs.7b02432.

(24) Niehaus, E.-M.; Kleigrewe, K.; Wiemann, P.; Studt, L.; Sieber, C. M. K.; Connolly, L. R.; Freitag, M.; Güldener, U.; Tudzynski, B.; Humpf, H.-U. Genetic Manipulation of the Fusarium Fujikuroi Fusarin Gene Cluster Yields Insight into the Complex Regulation and Fusarin Biosynthetic Pathway. *Chem. Biol.* **2013**, *20* (8), 1055–1066. https://doi.org/10.1016/j.chembiol.2013.07.004.

(25) Zhang, H.; Hantke, V.; Bruhnke, P.; Skellam, E. J.; Cox, R. J. Chemical and Genetic Studies on the Formation of Pyrrolones During the Biosynthesis of Cytochalasans. *Chem. – Eur. J.* **2021**, *27* (9), 3106–3113. https://doi.org/10.1002/chem.202004444.

(26) Heinemann, H.; Zhang, H.; Cox, R. J. Reductive Release from a Hybrid PKS-NRPS during the Biosynthesis of Pyrichalasin H. *Chem. – Eur. J.*, e202302590. https://doi.org/10.1002/chem.202302590.

(27) Hantke, V.; Skellam, E. J.; Cox, R. J. Evidence for Enzyme Catalysed Intramolecular [4+2] Diels–Alder Cyclization during the Biosynthesis of Pyrichalasin H. *Chem. Commun.* **2020**, *56* (19), 2925–2928. https://doi.org/10.1039/C9CC09590J.

(28) Bartlett, P. D.; Banavali, R. Spontaneous Oxygenation of Cyclic Olefins. Effects of Strain. *J. Org. Chem.* **1991**, *56* (21), 6043–6050. https://doi.org/10.1021/jo00021a016.

(29) Fujiyama, K.; Kato, N.; Re, S.; Kinugasa, K.; Watanabe, K.; Takita, R.; Nogawa, T.; Hino, T.; Osada, H.; Sugita, Y.; Takahashi, S.; Nagano, S. Molecular Basis for Two Stereoselective Diels–Alderases That Produce Decalin Skeletons**. *Angew. Chem. Int. Ed.* **2021**, *60* (41), 22401–22410. https://doi.org/10.1002/anie.202106186.

(30) Sato, M.; Kishimoto, S.; Yokoyama, M.; Jamieson, C. S.; Narita, K.; Maeda, N.; Hara, K.; Hashimoto, H.; Tsunematsu, Y.; Houk, K. N.; Tang, Y.; Watanabe, K. Catalytic Mechanism and Endo-to-Exo Selectivity Reversion of an Octalin-Forming Natural Diels–Alderase. *Nat. Catal.* **2021**, 4, 223-232. https://doi.org/10.1038/s41929-021-00577-2.

(31) Chi, C.; Wang, Z.; Liu, T.; Zhang, Z.; Zhou, H.; Li, A.; Jin, H.; Jia, H.; Yin, F.; Yang, D.; Ma, M. Crystal Structures of Fsa2 and Phm7 Catalyzing [4 + 2] Cycloaddition Reactions with Reverse Stereoselectivities in Equisetin and Phomasetin Biosynthesis. *ACS Omega* **2021**, 10. https://doi.org/10.1021/acsomega.1c01593.
(32) Guillén Schlippe, Y. V.; Hedstrom, L. A Twisted Base? The Role of Arginine in Enzyme-Catalyzed Proton Abstractions. *Arch. Biochem. Biophys.* **2005**, *433* (1), 266–278. https://doi.org/10.1016/j.abb.2004.09.018.
(33) Friedt, J.; Leavens, F. M. V.; Mercier, E.; Wieden, H.-J.; Kothe, U. An Arginine-Aspartate Network in the Active Site of Bacterial TruB Is Critical for Catalyzing Pseudouridine Formation. *Nucleic Acids Res.* **2014**, *42* (6), 3857–3870. https://doi.org/10.1093/nar/gkt1331.
(34) Hirokawa, T.; Boon-Chieng, S.; Mitaku, S. SOSUI: Classification and Secondary Structure Prediction System for Membrane Proteins. *Bioinformatics* **1998**, *14* (4), 378–379. https://doi.org/10.1093/bioinformatics/14.4.378.
(35) Bernhofer, M.; Dallago, C.; Karl, T.; Satagopam, V.; Heinzinger, M.; Littmann, M.; Olenyi, T.; Qiu, J.; Schütze, K.; Yachdav, G.; Ashkenazy, H.; Ben-Tal, N.; Bromberg, Y.; Goldberg, T.; Kajan, L.; O'Donoghue, S.; Sander, C.; Schafferhans, A.; Schlessinger, A.; Vriend, G.; Mirdita, M.; Gawron, P.; Gu, W.; Jarosz, Y.; Trefois, C.; Steinegger, M.; Schneider, R.; Rost, B. PredictProtein - Predicting Protein Structure and Function for 29 Years. *Nucleic Acids Res.* **2021**, *49* (W1), W535–W540. https://doi.org/10.1093/nar/gkab354.
(36) Wang, S.; Li, W.; Liu, S.; Xu, J. RaptorX-Property: A Web Server for Protein Structure Property Prediction. *Nucleic Acids Res.* **2016**, *44* (W1), W430-435. https://doi.org/10.1093/nar/gkw306.
(37) Attwood, M. M.; Krishnan, A.; Pivotti, V.; Yazdi, S.; Almén, M. S.; Schiöth, H. B. Topology Based Identification and Comprehensive Classification of Four-Transmembrane Helix Containing Proteins (4TMs) in the Human Genome. *BMC Genomics* **2016**, *17*, 268. https://doi.org/10.1186/s12864-016-2592-7.
(38) Beyer, E. C.; Berthoud, V. M. Gap Junction Gene and Protein Families: Connexins, Innexins, and Pannexins. *Biochim. Biophys. Acta BBA - Biomembr.* **2018**, *1860* (1), 5–8. https://doi.org/10.1016/j.bbamem.2017.05.016.
(39) Liu, S.; Li, S.; Shen, G.; Sukumar, N.; Krezel, A. M.; Li, W. Structural Basis of Antagonizing the Vitamin K Catalytic Cycle for Anticoagulation. *Science* **2021**, *371* (6524), eabc5667. https://doi.org/10.1126/science.abc5667.
(40) Shen, G.; Cui, W.; Cao, Q.; Gao, M.; Liu, H.; Su, G.; Gross, M. L.; Li, W. The Catalytic Mechanism of Vitamin K Epoxide Reduction in a Cellular Environment. *J. Biol. Chem.* **2021**, *296*, 100145. https://doi.org/10.1074/jbc.RA120.015401.
(41) Inaba, K.; Ito, K. Structure and Mechanisms of the DsbB-DsbA Disulfide Bond Generation Machine. *Biochim. Biophys. Acta* **2008**, *1783* (4), 520–529. https://doi.org/10.1016/j.bbamcr.2007.11.006.
(42) Malojčić, G.; Owen, R. L.; Grimshaw, J. P. A.; Glockshuber, R. Preparation and Structure of the Charge-Transfer Intermediate of the Transmembrane Redox Catalyst DsbB. *FEBS Lett.* **2008**, *582* (23–24), 3301–3307. https://doi.org/10.1016/j.febslet.2008.07.063.
(43) Guo, X.; Mayr, H. Quantification of the Ambident Electrophilicities of Halogen-Substituted Quinones. *J. Am. Chem. Soc.* **2014**, *136* (32), 11499–11512. https://doi.org/10.1021/ja505613b.

TOC graphic

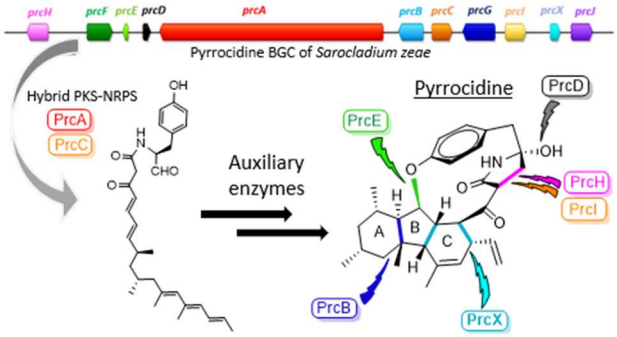
prcH
prcF
prcE
prcD
prcA
prcB
prcC
prcG
prcI
prcX
prcJ
Pyrrocidine BGC of Sarocladium zeae
Hybrid PKS-NRPS
PrcA
PrcC
Auxiliary
enzymes
Pyrrocidine
PrcD
PrcE
PrcH
PrcI
PrcB
PrcX
A
B
C
OH
CHO
HN
O
H